Journal of Visualization, Vol. 7, No. 1 (2004) 43-54

Analysis of Turbulent Premixed Flame Structure using Simultaneous PIV-OH PLIF

Cho, Y. *[1], Kim, J. -H. *[1], Cho, T. *[1], Moon, I.*[1], Yoon, Y.*[2] and Lee, C.*[3]

*1 School of Mechanical and Aerospace Engr., Seoul National University, Kwank-Gu, Seoul 151-742, Korea.
*2 School of Mechanical and Aerospace Engr., Seoul National University, Kwank-Gu, Seoul 151-742, Korea.
E-mail: ybyoon@snu.ac.kr
*3 Department of Aerospace Engineering, Konkuk University, Gwangjin-Gu, Seoul 143-701, Korea.

Received 26 March 2003
Revised 14 August 2003

Abstract : In the present study, we used a simultaneous PIV-OH PLIF measurement to acquire the strain rate and the chemical intensity and suggested a new combustion phase diagram. This simultaneous measurement was used to analyze the flame structure and to classify the combustion regimes of the opposed impinging jet combustor according to the change of the orifice diameters at the pre-chambers. The shear strain rates were obtained from the velocity measurement by PIV to represent flow characteristics and the OH radical intensities were obtained from OH PLIF to indicate the flame characteristics. When the strain rate and OH intensity at each point of the measurement zones are plotted at the strain rate-chemical intensity diagram, the distribution of each case showed the characteristics of each flame regime. The change of combustor condition made different distribution in the combustion phase diagram. As the orifice diameter of the pre-chamber decreases, well-mixed turbulent flames are produced and the combustion phase is moved from the moderated turbulence regime to the thickened reaction regime.

Keywords : simultaneous PIV-OH PLIF, opposed impinging jet combustor, Borghi diagram, the strain rate-chemical intensity diagram, combustion phase diagram, thickened reaction regime

1. Introduction

A structure of the turbulent premixed flames has been a subject of many previous studies. One branch of their study is to classify the combustion regimes on the basis of various criteria. In recent researches, it is found that the relations between the flow velocities and the chemical reaction rates play important roles in determining the mass consumption rate and reaction products (Broadwell and Lutz, 1998). Borghi (1984) suggested a combustion phase diagram classifying the turbulent combustion regimes. He categorized the turbulent premixed flames into several regimes based on measured values of turbulent intensities and integral length scales. Lipatnikov and Chomiak (2002) proposed modified Borghi diagram with the results of experimental investigations of flame quenching by intense turbulence. Lee et al. (1997) studied an opposed impinging jet combustor and classified the flames based on the Borghi's criteria. They used LDV to measure flow velocities and determined turbulent intensities and integral length scales. All previous researchers found that the correlation between flow field and the reaction field is significant, even though they could not provide

the correlations for the whole flow field.

Development of the laser diagnostics in the fluid mechanics enabled us to ok use simultaneous measurements of velocity and reaction intensity to analyze the turbulent flame structures. Rehm and Clemens (1998) applied simultaneous OH PLIF (planar laser-induced fluorescence) and PIV (particle image velocimetry) techniques and found good correspondence of high vorticity and strain rate regions with high OH concentration regions in a non-premixed flame issuing from a planar nozzle. Watson et al. (1999), using a simultaneous CH PLIF and PIV, found that the mean value of the total strain rate barely changes along the axial position. Han and Mungal (2000) used a simultaneous PIV-CH LIF method to measure the distribution of strain rate in the high *Re* diffusion flame front and found the transition from flame lift-off to flame blow-out. Kothnur et al. (2002) used a simultaneous PIV-OH/CH PLIF and found the relationship between kinematic quantities and high OH/CH region.

The goal of the present research is to suggest the idea of the new combustion diagram that can be equivalent to the Borghi diagram. Thus, we classified the turbulent premixed flames based on the strain rates and the OH intensities obtained from simultaneous PIV and OH PLIF measurements that can be implemented to the study of turbulent premised flame.

2. Experimental Apparatus and Method

2.1 Experimental apparatus and conditions

Figure 1 shows a schematic of a constant volume chamber with opposed dual pre-chambers having holes toward the center. The orifice size of the hole can be changed to 3mm, 4mm, and 5mm and the distance between each hole (H) is 35mm. According to Bray et al. (1996), the distance between two orifices has a large influence on turbulent strength. The diameter of main combustor is 120mm and the depth is 40mm. The volume of each pre-chamber is 67 cm^3. Each pre-chamber occupies 14.8 % of the total volume of the main chamber. Both of the pre-chamber and the main chamber are evacuated and then filled with propane-air mixture up to 1 atm. Two kinds of the equivalence ratio (ϕ= 0.85, 0.95) are used depending on the experimental purpose. The experimental condition is shown in Table 1.

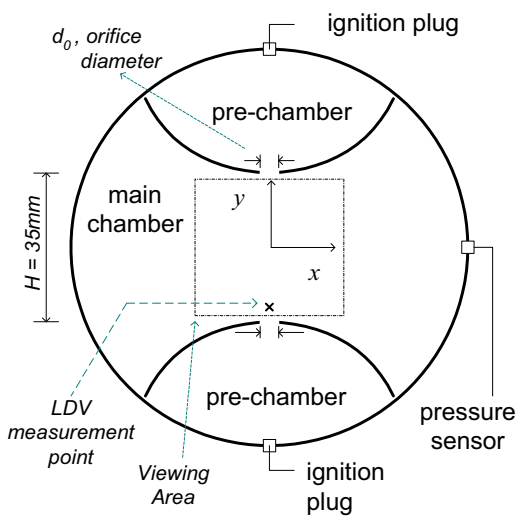

Fig. 1. Schematic of opposed impinging jet combustor.

Table 1. Experimental conditions and their flame regimes. Proper areas are selected from each image to analyze each flame regime. (Ext. indicates flame extinction)

Exp. Cases	Exp. Conditions	Selected Area	Flame Regime
A_{ext}	d_o = 3mm, ϕ=0.95	Q1	Flamelet Quenching
A	d_o = 3mm, ϕ=0.95	T1	Thickened Reaction Zone
B	d_o = 4mm, ϕ=0.95	M1	Moderate Turbulence
C	d_o = 5mm, ϕ=0.95	H2	High Turbulence
D	d_o = 4mm, ϕ=0.85	H1	High Turbulence
E	d_o = 5mm, ϕ=0.85	M2	Moderate Turbulence

2.2 Experimental setup for simultaneous PIV-OH PLIF

Figure 2 shows the experimental setup for PIV and OH PLIF measurements. The velocity field and the OH radical concentrations were measured simultaneously from the main chamber and the correlation between the flow property and chemical reaction was examined. As a laser system for the simultaneous measurements of the flow field, two Nd:YAG lasers (Spectra Physics GCR-170 and Continuum SureLite SSP) and a dye laser system (Lumonics HyperDYE-300 and Lumonics HyperTRAK-1000) were used.

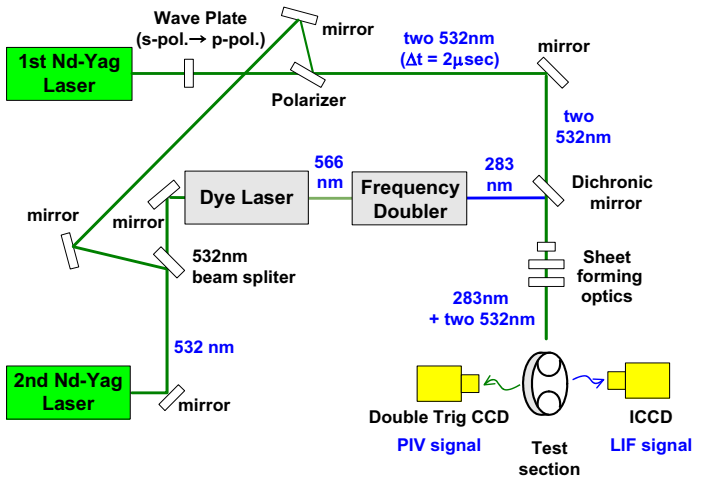

Fig. 2. Schematic diagram of the simultaneous PIV and OH PLIF diagnostics.

For PIV measurement, two second-harmonic beams (λ=532) are used. The beam of the second Nd:Yag laser is divided through the beam splitter. 30% of the power is used for PIV measurement and 70% of the power is used as a pumping laser to the dye laser for OH PLIF. The polarization of the first laser beam is changed from S-polarization to P-polarization through the wave plate and then combined with the second laser beam by a polarizing beam splitter (transmission: P-polarization, reflection: S-polarization). The combined beams are changed to sheet beams through the set of cylindrical lenses. A delay generator controls the time separation between two laser beams. The pulse separation is confirmed using a photo-diode and is fixed to 2 s. Scattering signals from seeding particles are recorded on a high resolution (1008×1018) Kodak ES 1.0 CCD camera (double trigger mode) equipped with f/2.8 AF Micro Nikkor 105 mm lens and 3× teleconverter for Nikon. The F-number of 105 mm lens is fixed to 5.6 during all experiments. The recorded area of scattering image is 21.45 mm × 21.65 mm. Velocity vectors are calculated by means of FFT-based cross-correlation technique. The delay generator controlled the opening time of the camera shutter for the synchronization with the laser pulse.

For OH PLIF measurements, the 532nm beam from the first Nd:YAG laser is changed to 567nm with the dye laser and this 567nm beam is changed to UV light (283.5nm) after it passes the frequency doubler. The output beam was minutely tuned to $Q_1(6)$ transition of the $A^2\Sigma^+ \leftarrow X^2(v'=1, v''=0)$ band (λ =282.93nm) and fluorescence from the A-X(1,0) and (0,0) bands (λ =306~320nm) was collected with a UV-Nikkor 105m f/4.5 lens. The image is focused onto the 640×480 ICCD camera (Stanford Computer Optics, 4Quik05). This camera was fitted with WG-305 and UG-11 color glass filters to reject scattering signal and incident light.

2.3 Borghi diagram and modified Borghi diagram

A structure of the turbulent premixed flame has been a subject of many previous studies. One branch of these studies is to classify the combustion regimes on the basis of various criteria. Figure 3a is the Borghi diagram that classified the turbulent reaction regimes. Figure 3b is the modified diagram where the regimes are classified based on the practical data by Lipatnikov and Chomiak (2002). In both diagram, L, δ_L, S_L and u' are the integral scale, the laminar flame thickness, the turbulent intensity and the laminar flame velocity, respectively. In the Borghi diagram, the combustion regimes are classified theoretically to 4 regimes (laminar flame, thickened flame, thickened wrinkled flame, wrinkled flame) with the dimensionless numbers, such as Re_t, Ka and Da. Borghi diagram is obtained based on the ideal academic assumptions (no heat losses; Le=1; equal molecular diffusivity et al.). The Ka=1 boundary, generally known as the Klimov-Williams criterion, separates the regimes

of wrinkled flame (thin reaction regime) from the thickened wrinkled flame (distributed reaction regime).

On the other hand, in the modified Borghi diagram, the combustion regimes are classified to 5 regimes (laminar flame, thickened reaction, flamelet quenching, moderate turbulence, weak turbulence) based on the experimental observations. The thickened reaction regime is also called the distributed reaction regime or the well-stirred reactor regime. This regime is related to the large turbulence intensity in the small length scale. It is a sufficient condition for this regime that the integral scale L is smaller than the laminar flame thickness δ_L ($L < \delta_L$). In this regime, the chemical reaction controlling the heat release occurs through all turbulence scale, but the occurrence is very limited due to the flame quenching (Lipatnikov and Chomiak, 2002; Chen, 1986; Chomiak and Jarosinski, 1982).

The moderate and weak turbulence regime can be called as various names: the wrinkled flame regime, the reaction sheet regime or the flamelet regime. The sufficient condition for these regimes is that the Kolmogrov scale η is much larger than the laminar flame thickness δ_L ($\eta >> \delta_L$). The reaction zone is wrinkled and occurs only in the thin area. This zone separates unburned reactants and burned products. The weak turbulence regime occurs when $u' \leq S_L$. The moderate turbulence regime occurs when $u' >> S_L$. In these regimes, the flamelet surface increased with the turbulence and the reaction zone is thicker than the integral length scale. The flamelet stretched by the turbulence may lead the local flame to extinction. In the moderate and weak turbulence regime, as the turbulence intensity increases, the reaction rate increases and the local flame extinction may occur when the turbulent intensity or strain rate is excessively high.

The experimental data from Lee et al. (1997) are plotted in Figs.3a and 3b and show their corresponding flame regimes. When the orifice diameter was decreased from 13mm to 5mm, the flame regimes moved from the weak turbulence regime to the moderate turbulence regime, which indicates that the flow characteristics can be influenced by the orifice diameter.

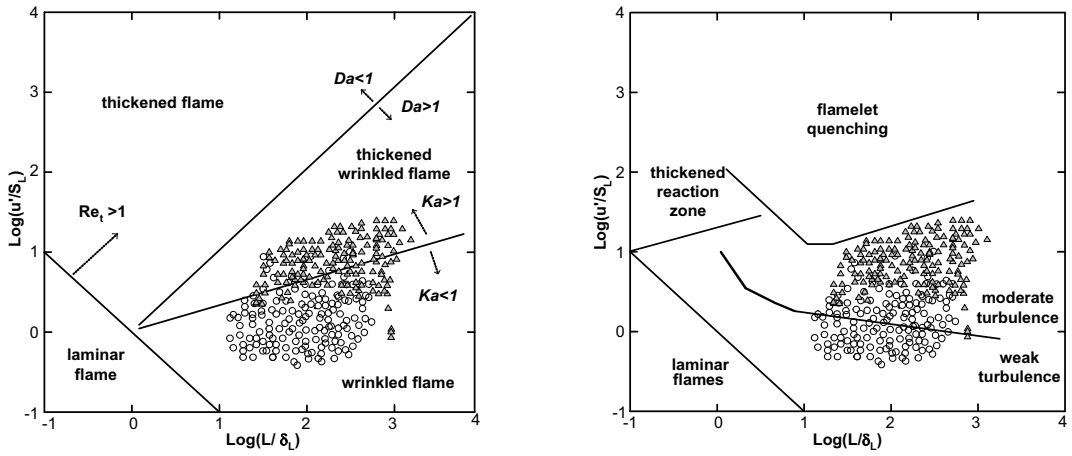

(a) Borghi diagram (b) Modified Borghi diagram

Fig. 3. Borghi diagram and modified Borghi diagram. The experimental data of Lee et al. (1997) are plotted at each diagram. (△: d_0=5mm, ϕ=0.95, ○: d_0=13mm, ϕ=0.95)

2.4 Major parameters for new diagram

Shear strain rate (ε)

Strain rates, which are represented by velocity gradient along x and y axis, indicate a degree of flow distortion and are intimately related with Karlovitz number which is a measure of flame stretch in the flow fields. Thus, the strain rate is one of the important parameters that represent the flame

structure characteristics. Strain rate (ε) is defined as Eqn. (1) and the discrete value of strain rate ($\varepsilon_{i,j}$) at each PIV data point is obtained by the formula according to Eqn. (2).

$$\varepsilon = \frac{\partial v}{\partial x} + \frac{\partial u}{\partial y} \tag{1}$$

$$\varepsilon_{i,j} = \frac{(v_{i+1,j-1} + 2\times v_{i+1,j} + v_{i+1,j+1})}{8h} - \frac{(v_{i-1,j-1} + 2\times v_{i-1,j} + v_{i-1,j+1})}{8h} + \frac{(u_{i-1,j+1} + 2\times u_{i,j+1} + u_{i+1,j+1})}{8h} - \frac{(u_{i-1,j-1} + 2\times u_{i,j-1} + u_{i+1,j-1})}{8h} \tag{2}$$

where u and v are the velocity components in x, y directions and h denotes a cell size.

Abdel-Gayed and Bredley (1989) found out that a shear strain rate breaks up the flame surface and then the flame disappears under stronger strains. Chen and Im (1998) reported that there is a close relation between the velocity of turbulent premixed flames and the stretch, and found that the stretch consists of a great portion of the shear strain rate. Darbiha et al. (1986) investigated the effect of the shear strain rate on premixed laminar flames and found that the shear strain rate extinguishes the flame partially. Bray et al. (1996) defined the bulk strain rate; $\varepsilon_b = V_{max}/H$, where V_{max} is the maximum jet velocity of the nozzle, and H is the distance between nozzles, and they found that the bulk strain rate is an important parameter to extinguish the opposed impinging flames. Thus, we measured the shear strain rate as a representative value of a flow property by varying the orifice diameter of the pre-chamber from 3 to 5 mm. As the orifice diameter decreases, the strain rates increase and causes flames to be extinguished.

OH signal intensity (σ)

OH PLIF was used to obtain spatially and temporally resolved images of the reaction zone in the opposed impinging jet combustor. The OH radical concentration increases rapidly around the flame for 20μsec and then decomposes slowly in 1 to 5 ms by a 3-body recombination reaction (Seitzman et al., 1990). Thus, near the flame front exists supereqilibrium OH. The OH radical, that is intermediate product of chemical reaction, has a concentration which is ten times higher than that of O or H radicals (Turns, 1996). Therefore, the OH radical is found to emit more intensive fluorescence signal than other species when they absorb the laser light. Hence, the fluorescence signal of OH radical is widely used as an indicator of flame front in reacting flows.

Strain rate – chemical intensity relation

Borghi diagram and modified Borghi diagram have been used to classify the turbulent reaction regimes. In both diagrams, the characteristic velocity (u'/S_L) and the characteristic flame length (L/δ_L) are used as parameters (Lipatnikov and Chomiak, 2002). Assuming the values are fixed in case the type of combustible gases and initial conditions are determined (Lee et al., 1997), the laminar flame thickness (δ_L), and the laminar flame velocity (S_L) have constant values. Usually the values of the integral scale (L) and the turbulent intensity (u') can be obtained from the point measurements such as LDV, and the calculated values (u'/S_L, L/δ_L) can be plotted at the combustion diagram. However, in the unsteady phenomenon, a point measurement cannot provide full information for the whole flow field.

In this study, we selected strain rate and chemical intensity as parameters and suggested a new diagram using these parameters. Recent advance in the laser diagnostics such as the simultaneous PIV-OH PLIF enabled us to obtain the strain rate and chemical intensity simultaneously at the whole flow field. The turbulent reaction regimes were analyzed based on the correlations between two variables in each combustion phenomenon. The correlations depended on the combustion phase and flame structure. We used the same combustion regime name defined in the modified Borghi diagram because the location of each combustion regime on a new combustion diagram can be related to that on the Borghi diagram. This strain rate-chemical intensity diagram is a convenient diagram in a sense that it can be obtained from the laser diagnostics with simple calculations and explained with relation to the classification of modified Borghi diagram.

3. Results and discussion

3.1 Characteristics of the impinging jet combustor

At the previous research on the opposed impinging jet combustor, the velocity and stain rate were measured to clarify the mechanism of NOx reduction through the PIV technique (Lim et al., 2000). They found a highly strained velocity field in the main combustor when small diameter orifice was used at the pre-chambers. The ejected flow from the pre-chamber made highly turbulent flow field and restricted the chemical reaction within the main combustor. This reaction-restricted stage is called as ignition delay. Due to the ignition delay, the total period for combustion is reduced and the intense combustion occurred within relatively short period. When the smallest diameter orifice was applied, the combustion time was reduced by more than 30% compared with the larger diameter case. While maintaining the pressure increase at the same level of the conventional combustor without pre-chamber, they reduced the NOx emission substantially by a factor of 1/2 through the shortened reaction time and well-distributed reaction. The reduction of NOx emission can be attributed to the enhancement of the intermolecular mixing between cold and hot spots in highly turbulent flows.

Figure 4 shows the characteristics of combustion process in the opposed impinging jet combustor. The Schilieren photographs were taken using the high-speed camera (40,000 frames/sec). At first the premixed gas in the pre-chamber is ignited and then expanding combustion gas induces highly strained flows. The ejected jets make stagnation plane and then the global reaction occurs in the main combustor. This figure is obtained from the condition of d_0=5mm, Φ=0.95 at the same geometry of the combustor (Lee et al., 1997). The histories of chamber pressure and ejection velocity are shown in the following Fig. 5 and the four dots on the pressure curve of this figure denote the time locations when the schilieren images were taken.

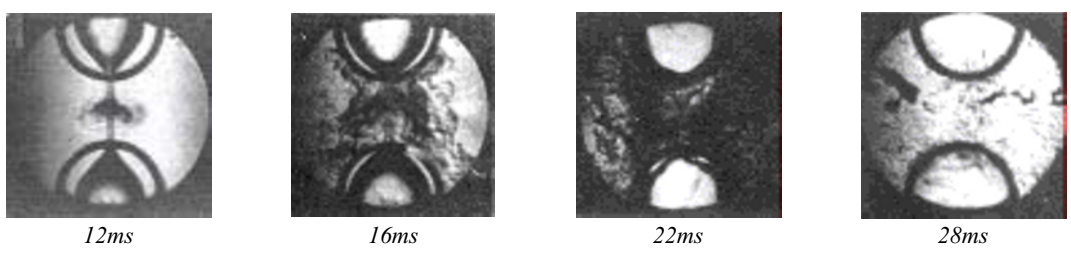

Fig. 4. Schlieren photographs of opposed impinging combustor. (d_0 = 5mm, Φ = 0.95)

3.2 Pressure curves of the impinging jet combustor

From the measured pressure data using Piezo-resistive sensors, we found that the pressure history could be divided into three regions: jet flame ejection period, main combustion period and post-combustion period as shown in Fig. 5. It is noted that the peak pressure during the main combustion reaches 7 bars (main combustion period) and the pressure immediately falls down to 2-3 bars and then the pressure reaches 5 bars (post-combustion period). This means that the flammable gas mixture in the main chamber is not burned completely during a main combustion period so that the remaining unburned mixture is burned during a post-combustion period. It is found that the post-combustion period is longer than the main combustion period.

Figure 5 is the time histories of the ejection velocity and the chamber pressure that are measured at the 5mm above the orifice of pre-chamber (LDV measurement point at Fig.1) and at the wall of the main chamber (pressure sensor in Fig.1), respectively. This figure explains the motion of flow field in the opposed impinging jet combustor after the dual ignitions inside of the pre-chambers. After the ignition, the expanding hot gas inside the pre-chambers is ejected into the main chamber through small orifices. The high-speed jets are collided at the middle of main combustor and then

generate strong turbulent flows. During this jet flame ejection period, the ejection velocity increases and stays at maximum velocity (45m/s). However, in this period the collision of the two jets are not immediately followed by the main combustion. As shown in Fig. 5, only small pressure increase is observed during the ignition delay. We defined the *ignition delay* when the chamber pressure increases to 10% of maximum pressure difference and this is used as a boundary between the jet flame ejection and the main combustion period. At this time the velocity and the chemical signal were obtained by the simultaneous PIV-OH PLIF measurement. In this ejection period, the unburned gas can be mixed with the hot gas jet and this process generates high turbulence inside the chamber. After the ignition delay the premixed gas in the main chamber is ignited and reaches its maximum pressure value.

Figure 6 indicates the pressure history of each case. The orifice diameter of the pre-chamber and the equivalence ratio of premixed gas affect the ignition delays of main combustion. It is very interesting to notice the different consequences found in cases A and A_{ext}. These two cases have same experimental condition (d_0 = 3mm and ϕ = 0.95) and the same flow characteristic during the delay time. However, their flames in main chamber is found at two distinct combustion phases: flamelet quenching or thickened reaction. At this critical point, the intensively strained flow field can be followed by both the flame extinction and the re-ignition. For d_0=4, 5mm cases, the ignition delay decreases as the equivalence ratio (ϕ) increases because higherϕ provides a faster chemical reaction. However, the maximum pressure (P_{max}) values do not show consistency. As ϕincreases, P_{max} increases in d_o =4mm case but decreases in d_o =5mm case. This phenomenon shows that the turbulent flames are affected not by the chemical reaction rate but by the interactions of chemistry and flow characteristics.

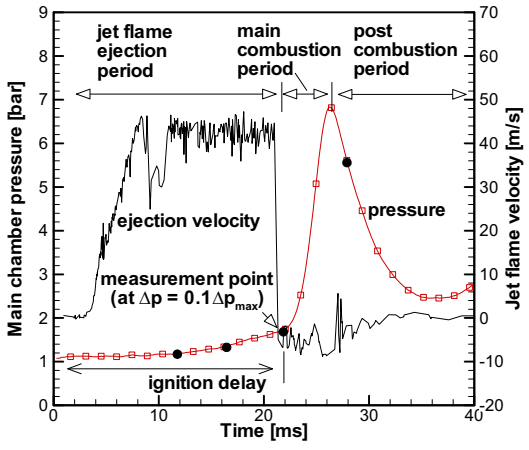

Fig. 5. Time histories of pressure and ejection velocity (d_0 = 5mm, ϕ = 0.95).

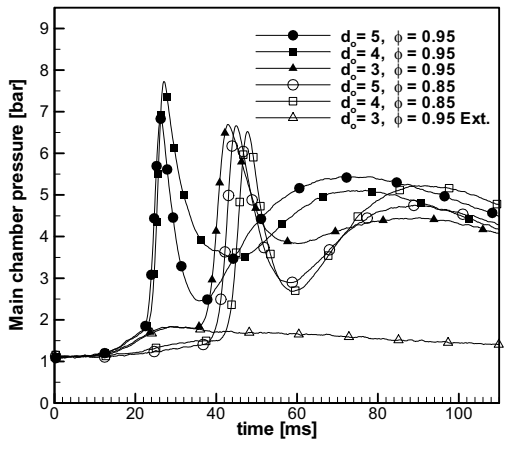

Fig. 6. Pressure histories for each condition in main chamber.

3.3 Shear strain rates and OH intensities

Figure 7 is overlapped images of strain rate and OH intensity obtained by the simultaneous PIV-OH PLIF measurements. Those images were taken from the viewing area located at the center of the main as shown in Fig.1. The line contours and the numbers indicate strain rates(ε) and the color backgrounds represent the OH intensity(σ). In each case, we selected some sub-regions that represent flamelet quenching, thickened reaction zone, high turbulence and moderate turbulence regime. In Fig. 8 the strain rate and OH intensity are plotted for each regime that is the size of 8mm×8mm. The strain rates and OH intensities from the sub-regions, named as Q1, T1, M1, M2, H1, and H2 as shown in Table 1, are compared with each other in order to find any trends corresponding

to the regimes in the modified Borghi diagram. As mentioned previously, the interactions of turbulence and reaction not only promote the chemical reaction but also lead to flame quenching. Thus, in order to investigate the relation between turbulence and reaction, we selected strain rates (ε) and OH intensity (σ) as representative parameters of flow and flame characteristics, and then found the relation between an OH intensity and a strain rate for each case corresponding to a specific regime in the modified Borghi diagram.

Flame extinction case is shown in Fig. 7a where OH intensities are low although high strain rate regions exist. In this case the premixed gas is ignited in the pre-chamber and the burned hot gas is ejected to the main chamber, but the phenomenon in the main chamber may undergo re-ignition (thickened reaction) or extinction (flamelet quenching) because this condition is close to the border line between flame extinction and re-ignition. In Fig. 7b, thickened reaction regime can be found, where strong turbulence is observed and flames are thickened by small eddies (Lipatnikov and Chomiak, 2002). This regime can be quenched easily under some highly strained conditions. Although the images in Figs. 7a and 7b were obtained under the identical conditions (d_o=3mm, ϕ=0.95), the results are not identical; it may result in the thickened reaction or flame let quenching. As shown in the strain rate-OH intensity diagram in Figs .8a and 8b, the general trends of flow field are similar to the fact that the strain rates are distributed widely. However, the maximum values of strain rates in the thickened flame region are larger than those in the flame quenching. The reason may be due to the fact that chemical reactions of the thickened reaction case locally add more energy to turbulence and increase turbulence intensity.

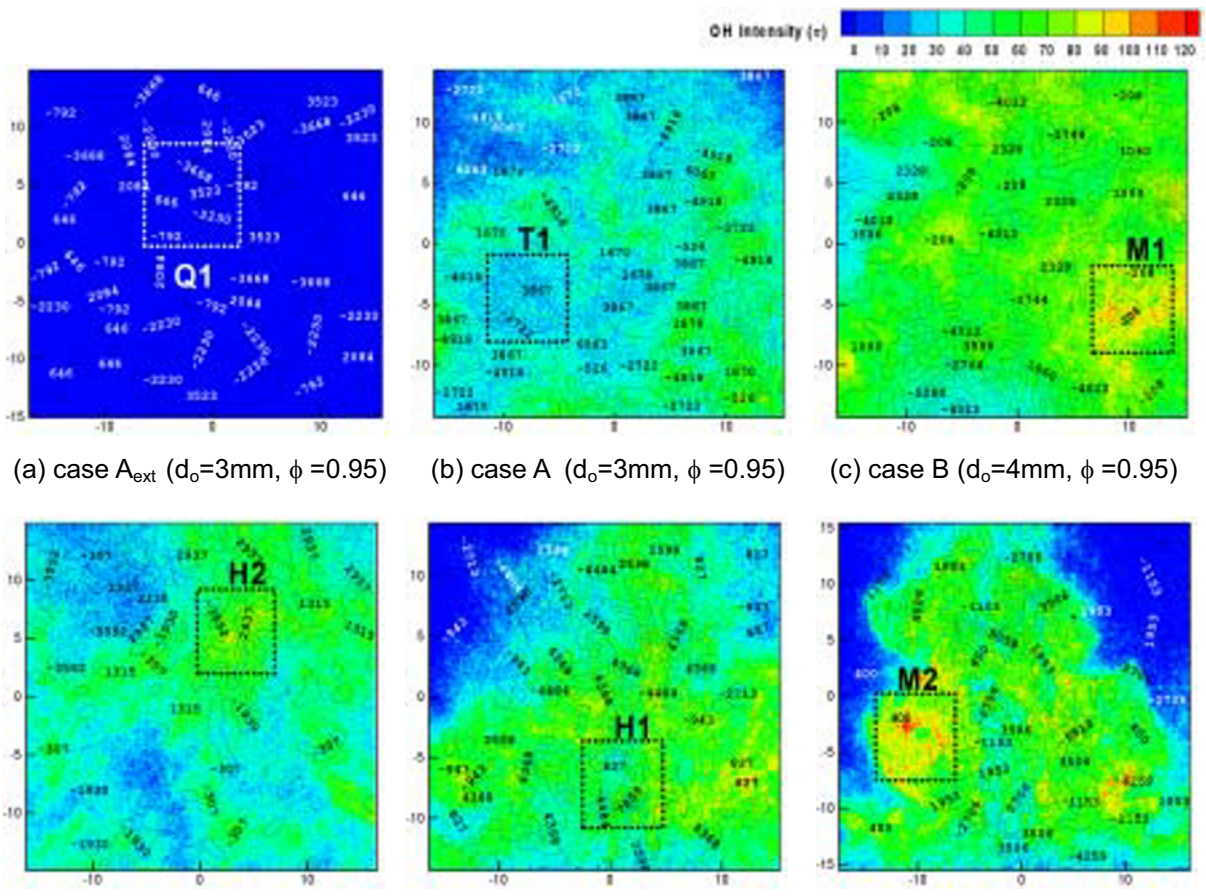

(a) case A_{ext} (d_o=3mm, ϕ =0.95) (b) case A (d_o=3mm, ϕ =0.95) (c) case B (d_o=4mm, ϕ =0.95)

(d) case C (d_o=5mm, ϕ =0.95) (e) case D (d_o=4mm, ϕ =0.85) (f) case E (d_o=5mm, ϕ =0.85)

Fig. 7. Images of strain rates and OH intensities from simultaneous PIV-OH PLIF measurements.

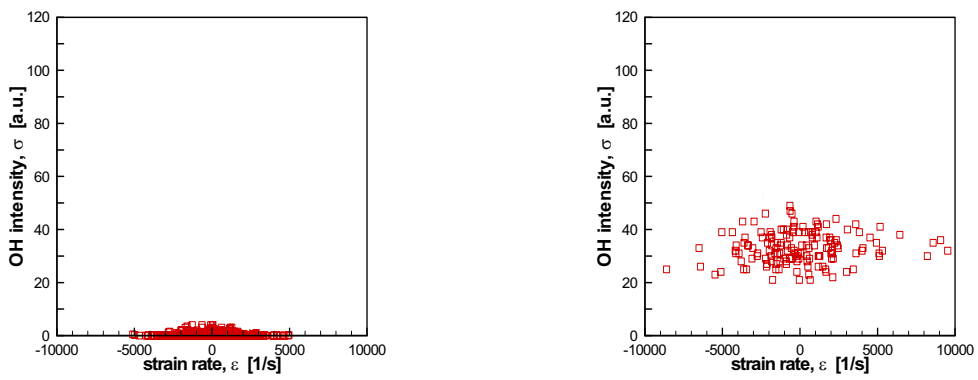

(a) flamelet quenching, area Q1 at case A_{ext} (b) thickened reaction zone, area T1 at case A

(c) high turbulence, area H1 in case D (d) moderate turbulence, area M2 in case E

Fig. 8. Strain rates and OH intensity distributions for the regimes in modified Borghi diagram.

The moderate turbulence regimes shown in Figs. 7c and 7f appear very often in practical systems according to Lipatnikov and Chomiak (2002). The strain rates of this regime have lower values and vertically scattered as shown in Fig.8d, which is different from the cases of the thickened reaction and flame quenching. Figs. 7d and 7e show high turbulence regime. In this regime, the values of strain rate and OH intensity are scattered widely as shown in Fig. 8c.

3.4 The strain rate-chemical intensity diagram

We calculated the turbulence intensities of selected areas (Q1, T1, H1, H2, M1 and M2) in Fig.7 and plotted the characteristics of each case in the modified Borghi diagram as shown in Fig.9. In general, time averaged values are required to determine the turbulence. However, it is impossible to obtain the time averaged values in this research because the velocity values obtained from PIV measurement are instantaneous values in the transient process of this combustor. However, if we assumed that the flow field of 8mm×8mm is homogeneous for the short period of time, the turbulent intensity can be obtained as follows;

$$u' \cong u - \langle u \rangle_{volume} \text{ where } \langle u \rangle_{volume} \cong \langle u \rangle_{time} \tag{3}$$

The small value is selected as the integral scale L between the longitudinal length scale and lateral length scale as shown in Eqns (4) and (5), respectively. Also, the volume-averaged values are used instead of time-averaged value to correlate turbulent intensity.

$$\textit{Longitudinal length scale: } L_{\alpha\alpha}^{\alpha} = \frac{1}{\langle u'_{\alpha}(\vec{x}) u'_{\alpha}(\vec{x}) \rangle_{time}} \int_0^{\infty} \langle u'_{\alpha}(\vec{x}) u'_{\alpha}(\vec{x} + r_{\alpha}) \rangle_{time} \, dr_{\alpha} \tag{4}$$

$$\textit{Lateral length scale: } L_{\alpha\alpha}^{\beta} = \frac{1}{< u'_{\alpha}(\vec{x}) u'_{\alpha}(\vec{x}) >_{time}} \int_{0}^{\infty} < u'_{\alpha}(\vec{x}) u'_{\alpha}(\vec{x} + r_{\beta}) >_{time} dr_{\beta} \tag{5}$$

$$\text{where } < u'u' >_{time} \cong < u'u' >_{volume}$$

Especially, the combustion regime of this research is concentrated at the thickened reaction zone and the moderated turbulence zone.

Figure 10 shows a flow-chemistry diagram that is a newly suggested combustion diagram for the turbulent premixed flame based on strain rates and OH intensities. All values shown in Fig. 8 are plotted in Fig.10. The strain rates and OH intensities are normalized by bulk strain rate ($\varepsilon_b = V_{max}/H$) and maximum OH intensity (σ_{max}), respectively.

As shown in Fig.9, the turbulence zone in the diagram can be divided into four regimes (thickened reaction regime, weak turbulence regime, moderate turbulence regime, flamelet quenching regime) and the selected areas in table 1 ranges from the moderated turbulence regime to the thickened reaction regime. The weak turbulence regime cannot be found in this diagram because the weak turbulence occurs only when the orifice size d is larger than 5mm (Lee et al., 1997). Our experiments are limited from d_o= 3mm to d_o=5mm cases. We found some difficulties to classify the regimes distinctly. Especially, there are some overlapped regions between moderate turbulence and thickened reaction although flame quenching and weak turbulence are classified effectively.

The high turbulence regime has lower OH signal intensity than that of the moderated turbulence regime as shown in Fig. 8c and 8d. The reason is that the wrinkle of flame is broken into pieces and results in the flame extinction when $\log(u'/S_L)$ value is over 1 as shown in Fig. 9. Thickened reaction regime is the intermediate regime between the flame of geometric structure and the flame quenching. This phenomenon is found in this research although it is not easy to be detected. In this regime, the OH signal intensity decreases but the strain rate increases as shown in Fig. 8b. In case of quenching condition, the OH signal decreases significantly, but the strain rate is maintained. The regimes of flamelet quenching (flame extinction) show bell-shape graph as shown in Fig. 8a. In the present research the idea of the strain rate-chemical intensity diagram is suggested and that diagram may be used as an equivalence to the Borghi diagram. This diagram classifies each combustion regimes and shows the dependency between chemical intensity and strain rate of each combustion regime.

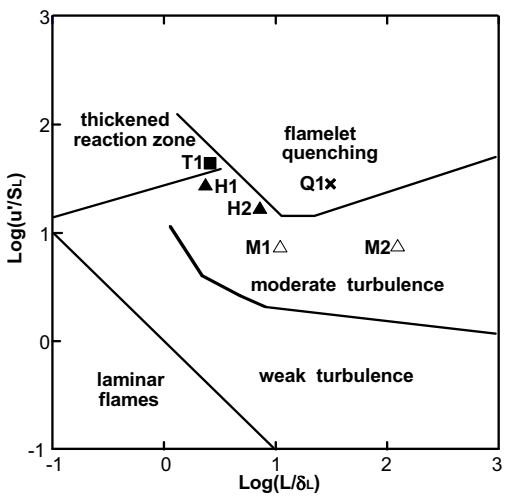

Fig. 9. Combustion phases of selected cases in the modified Borghi diagram.

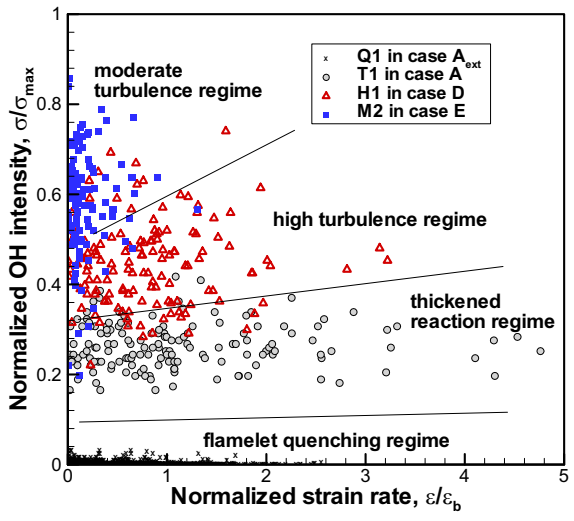

Fig. 10. Strain rate–chemical intensity diagram based on strain rates and OH intensities.

4. Conclusions

In a constant volume combustor, we made the opposed impinging jet flame using dual pre-chambers with premixed propane-air gas and measured its characteristics with the simultaneous PIV-OH PLIF measurements. When the orifice diameter is decreased, the speed of turbulent flame and the ignition delay increases. Thus, with the small orifices were used, the sufficiently well mixed turbulent flames are produced by homogeneously spreading radicals in the chamber when the re-ignition occurred. Furthermore, the flame is quenched partially due to the high strain rate.

The turbulence combustion cannot be explained solely by either flow or chemical characteristics. Both effects should be considered. We suggested the strain rate-OH intensity diagram as a new practical diagram that is easily obtained from the simultaneous PIV-OH PLIF measurements. The turbulence characteristics are replaced with the strain rate and the chemical characteristics are represented by the OH signal intensity. We categorized the combustion phases of the opposed impinging jet combustor at the various orifice diameters. This new diagram classified turbulent premixed flames effectively based on flame structures.

Acknowledgments

This work was supported by grant M1-0104-00-0058 from the National Research Laboratory program of the KISTEP (Korea Institute of Science & Technology Evaluation and Planning). This support is gratefully acknowledged.

References

Abdel-Gayed, R. G. and Bradley, D., Combustion Regime and Straining of Turbulent Premixed Flame, 1989, Combust. Flame, 78 (1989), 213.

Borghi, R., On the Structure of Turbulent Premixed Flames, Recent Advance in Aeronautical Science (Bruno, C. & Casc, C., Eds), Pergamon, (1984).

Bray, K. N. C., Champion, M. and Libby, P. A., Extinction of Premixed Flames in Turbulent Counterflowing Streams with Unequal Enthalpies, Combust. Flame, 107 (1996), 53.

Broadwell, J. E. and Lutz, A. E., Combust. Flame, 114 (1998), 319.

Chen, J. H. and Im, H. G., Correlation of Flame speed with Stretch in Turbulent Premixed Methane/Air Flames, Proc. Combust. Inst., 27 (1998), 819.

Chomiak, J. and Jarosinski, J., Flame Quenching by Turbulence, Combust. Flame, 48 (1982), 241.

Darabiha, N., The Effect of Strain Rate on a Premixed Laminar Flame, Combust. Flame, 64 (1986), 203.

Friedlander, S. K., Smoke, Dust, and Haze 2nd ed., Oxford New York, (2000), 222.

Han, D. H and Mungal, M. G., Simultaneous Measrement of Velocity and CH Layer Distribution in Turbulent Non-Premixed Flames, Proc. Combust. Inst, 28 (2000).

Kostiuk, L. W., Bray, K. N. C. and Cheng, R. K., Experimental Study of Premixed Turbulent Combustion in Opposed Streams. Part Ⅱ, Combust. Flame, 92 (1993), 396.

Kothnur, P. S, Tsurikov, M. S., Clemens, N. T., Donbar, J. M. and Carter, C. D., Planar Imaging of CH, OH and Velocity in Turbulent Nonpremixed Jet Flames, Proc. Combust. Inst., 29 (2002).

Lee, H. G., Jeung, I. -S. and Yoon, Y., An Experimental Study on NOx Reduction by the Opposed Impinging Jet Flames, The First Asia-Pacific Conference on Combustion, Osaka, Japan, May 1997.

Lim, S., Yoon, Y., Lee, C. and Jeung, I. -S., Effect of Strain Rate on NOx Reduction in Opposed Impinging Jet Flame Combustor, 10th Int'l Symposium on Applications of Laser Techniques to Fluid Mechanics, Lisbon, Portugal, July 2000.

Lipatnikov, A. N. and Chomiak, J., Turbulent Flame Speed and Thickness, Prog. Energy Combust. Sci., 28 (2002), 1.

Rehm, J. E and Clemens, N. T., The Relationship Between Vorticity/Strain and Reaction Zone Structure in Turbulent Non-Premixed Jet Flames, Proc. Combust. Inst., 27 (1998), 1113.

Seitzman, J. M., Ungut, A., Paul, P. H. and Hanson, R. K., Imaging and Characterization of OH Structure in a Turbulent Nonpremixed Flame, *Proc. Combust. Inst.,* 23 (1990), 637.

Turns, S. R., *An Introduction to Combustion*, MacGraw-Hill, New York (1996).

Watson, K. A., Lyons, K. M., Donbar, J. M. and Carter, C. D., Scalar and Velocity Field Measurements in a Lifted CH_4-Air Diffusion Flame, Combustion Flame, 117 (1999), 257.

Author Profile

Yongjin Cho: He received his MS degree in School of Mechanical and Aerospace Engineering in 2002 from Seoul National University. His research interests are laser diagnostics such as simultaneous PIV and PLIF, bluff-body stabilized supersonic flame and turbulent flame in the opposed impinging jet combustor.

Ji-Ho Kim: He received his Ph. D degree and MS degree in School of Mechanical and Aerospace Engineering at Seoul National University in 2003 and 1998, respectively. His research interests are laser diagnostics such as simultaneous PIV and PLIF, bluff-body stabilized supersonic flame, and numerical simulation for model scramjet engine.

Taeyoung Cho: He is a master candidate in School of Mechanical and Aerospace Engineering at Seoul National University. His research interests are laser diagnostics such as simultaneous PIV and PLIF, bluff-body stabilized supersonic flame.

Insang Moon: He received MS degree from Department of Astronomy at Yonsei University in 1988 majoring in optimum orbit transfer and ME degree from Department of Aerospace Engineering in 1998 at University of Michigan and Ph. D degree from the same University in 2003 majoring in heterogeneous combustions. Currently, he is in Post Doctoral course of Seoul National University researching laser diagnostics, such as PIV and PLIF, and NOx reduction in a small combustor.

Youngbin Yoon: After MS degree in Department of Aerospace Engineering in 1987 at Seoul National University, he received Ph. D degree in Department of Aerospace Engineering in 1994 at University of Michigan. After obtaining Ph. D, he worked as a researcher in University of California, Davis. And then he joined Seoul National University and currently is an associate professor. His research interests are visualization, laser diagnostics, supersonic combustion, turbulent diffusion flames and liquid rocket injectors.

Changjin Lee: After MS degree in School of Mechanical and Aerospace Engineering in 1985 at Seoul National University, he received Ph. D degree in Department of Aeronautical & Astronautical Engineering in 1992 at University of Illinois at Urbana-Champaign. He joined as a faculty of Department of Aerospace in Konkuk University and currently is professor. His research interests are flame instability, hybrid combustion, and solid propellant combustion modeling.